Analysis and Design of a Planar Multilayered FSS with Arbitrary Incidence

[1]L. Latrach, [1]N. Sboui, [1]A. Gharsallah, [1]A. Gharbi, and [2]H. Baudrand

[1] Laboratoire d'Electronique Département de physique Faculté des sciences de Tunis, 2092 El Manar Tunisia
E-mail : noureddine.sboui@fst.rnu.tn
[2] Laboratoire d'Electronique EN SEEIHT de Toulouse France

Abstract – A rigorous technique based on the transverse Wave Concept Iterative Procedure (WCIP) and a Fast Mode Transformation (FMT) is used to analyze the Frequency Selective Surface (FSS). These structures are used as filters and reflector antenna as well as deep-space exploration for multi-frequency operations. In order to initialize the iterative procedure, an incident wave is defined in spatial domain with arbitrary angle of incidence. The numerical complexity is studied and compared to the classical MoM. The good agreement between simulated and published data justifies the design procedure.

Keywords: Arbitrary incidence, single-layer, multilayered, and 2D-FFT algorithm.

I. INTRODUCTION

Frequency Selective Surface structures have played an important role in the recent development of antennas and microwave device technology. They are used as spatial filters [1], artificial surfaces [2] and a deep- space exploration for multi-frequency operations [3]. Typically, FSS structures consist in two-dimensional periodic resonant element supported by one or multilayer of dielectrics. Performances depend on their substrate characteristics, element type, dimensions and the spacing between elements.

To design the FSS arrays, a number of analytical and numerical techniques has been developed. One of the most popular is the Method of Moments (MoM) and its derivatives [4-6]. Yet, one can compute the unknown current distribution on the FSS screens in one-step. Then the small dimensions of the circuit cause some problems in result precisions thus coupling conditions between the different elements must be taken into account. The Mode Expansion Method [7] and the Spectral-Domain Method [8] have been developed to analyze the FSS structures. However, the efficiency, memory consumption and time requirement usually make these methods unsuitable for optimization. For its simplicity, the Equivalent- Circuit Method is used to design the FSS structures [9-10], but its application is limited only for known simple forms [9].

During the last few years, the FMT-WCIP method has been applied in wide variety of microwave structures [11-13]. It consists in successive reflections between the FSS screens and their two sides. It has also an alternative behavior between space and spectral domains. There are several procedures to change wave domains. In [14], The Galerkin technique is used. In each stage of analysis, the transformation passage from spatial to spectral (and vice versa) is long. As in [11-13], we combine the wave concept with the 2D-FFT algorithm to change the domain. The use of the 2D-FFT algorithm is required to mesh the circuit plane into 2D small rectangular cells. Hence, the boundary conditions are satisfied at each cell. By using the 2D-FFT algorithm, a high computational speed can be achieved. This method is simple since it involves neither basic functions nor matrix inversion. Thus, it not only over comes the limitation of the above methods, but it is also suitable for general structure. In [11-13], the circuit under studied is deposed on one dielectric layer surrounded by four perfect electric walls, and is defined in the spatial domain. The source excitation consists in an electric filed E0 placed between the circuit and an electric wall of the cavity. In reference [15], the WCIP is used to study a stratified isotropic/anisotropic FSS structure with a normal incidence angle.

The purpose of this paper is to extend the Wave Concept Iterative Process method WCIP to the analysis of a Frequency Selective Surfaces FSS structures with an arbitrary incident angle in the multilayer configuration. The numerical complexity of the iterative procedure is studied and compared to the classical MoM. Two different examples are studied; single simple layer and multilayer. For the two cases, our simulated results are validated with those of other methods and measurements.

II. THEORY

Let us consider a periodic arbitrary multilayer structure, as shown in Fig. 1. Figure 2 shows the unit cell at the Ω_i interface. This interface can support the circuit and includes two sub-domains Metal M_i and Dielectric D_i. We suppose that the electromagnetic field is known

on all points of the interface plane. The solution of the problem has to satisfy the following boundary conditions,

$$\begin{cases} E_{T\,i} = E_{T\,(i+1)} = 0 \quad On \quad M_i \\ H_T = H_{T\,i} + H_{T\,(i+1)} \quad On \quad D_i \ . \end{cases} \tag{1}$$

In the last equation, E_{Ti} and $E_{T(i+1)}$ are respectively, the spatial tangential components of the electric field at medium *i* and *(i+1)* with H_{Ti} and $H_{T(i+1)}$ as their corresponding magnetic fields.

The wave concept is introduced by writing the tangential electric and magnetic fields (E_{Ti},H_{Ti}) in terms of incident (A_i) and reflected (B_i) waves, as shown in Fig. 3 [13]. It leads to the following equation,

$$\begin{vmatrix} A_i \\ B_i \end{vmatrix} = \frac{1}{2\sqrt{y_{0i}}} \begin{vmatrix} y_{0i} & 1 \\ y_{0i} & -1 \end{vmatrix} \begin{vmatrix} E_{T\,i} \\ H_{T\,i} \wedge n_i \end{vmatrix}. \tag{2}$$

The symbol n_i is the unit vector orthogonal to Ω_i giving the direction of the incident and reflected waves and y_{0i} is an intrinsic admittance characterizing the medium. It is often chosen as $\sqrt{\varepsilon_0 \varepsilon_{ri} / \mu_0}$ in which ε_0, μ_0 and ε_{ri} are respectively, the permittivity and permeability of the vaccum and the relative permittivity of the medium 'i'.

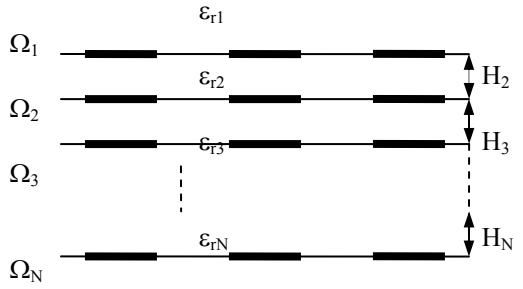

Fig. 1. General periodic multilayer structure.

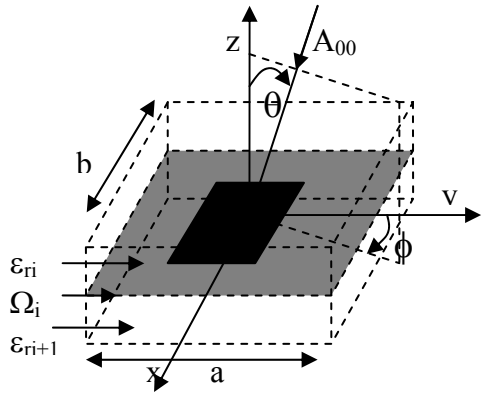

Fig. 2. Unit cell of the periodic structure with arbitrary incidence A_{00}.

This last equation allows us to write the boundary conditions given by equation (1) as the following general spatial equation,

$$\begin{vmatrix} B_i \\ B_i^{'} \end{vmatrix} = \left\{ \underbrace{\left[\hat{S}_{M\,i} \right] + \left[\hat{S}_{D\,i} \right]}_{[\hat{S}_i]} \right\} \cdot \begin{vmatrix} A_i \\ A_i^{'} \end{vmatrix} \tag{3}$$

$$\left[\hat{S}_{Di} \right] = \frac{\hat{H}_{Di}}{1+n_{0i}^2} \begin{vmatrix} 1-n_{0i}^2 & 2n_{0i} \\ 2n_{0i} & n_{0i}^2 - 1 \end{vmatrix},$$

$$n_{0i} = \sqrt{\frac{y_{0i+1}}{y_{0i}}}, \quad \left[\hat{S}_{M\,i} \right] = \begin{vmatrix} -1 & 0 \\ 0 & -1 \end{vmatrix}.$$

and $$\hat{H}_{\pi} = \begin{cases} 1 \ \ if \ \ \pi = M_i \ \ or \ \ D_i \\ 0 \ \ else \ where \end{cases}$$

Hence, we deduce the global spatial equation relating the reflected waves to the incident ones on all the interfaces,

$$\left\{ \begin{vmatrix} B_1 \\ B_1^{'} \\ B_2 \\ B_2^{'} \\ \vdots \\ B_i \\ B_i^{'} \\ \vdots \\ B_N \\ B_N^{'} \end{vmatrix} = \begin{vmatrix} [S_1] & & & & & & \\ & [S_2] & & & & & \\ & & \ddots & & & & \\ & & & [S_i] & & & \\ & & & & \ddots & & \\ & & & & & [S_N] & \end{vmatrix} \begin{vmatrix} A_1 \\ A_1^{'} \\ A_2 \\ A_2^{'} \\ \vdots \\ A_i \\ A_i^{'} \\ \vdots \\ A_N \\ A_N^{'} \end{vmatrix} \right\}_{x,y} . \tag{4}$$

Between two consecutive interfaces (*i* and *i+1* for example), the waves are defined in the spectral domain (TE and TM modes), and are led by the following spectral equation, Fig. 3.

$$\left\{ \begin{vmatrix} A_i^{'} \\ A_{i+1} \end{vmatrix} = \left[L_{i+1} \right] \begin{vmatrix} B_i^{'} \\ B_{i+1} \end{vmatrix} \right\}_{TE,TM}, \tag{5}$$

$$\left[L_{i+1} \right]_{\alpha} = \begin{bmatrix} l_{1\alpha} & l_{2\alpha} \\ l_{2\alpha} & l_{1\alpha} \end{bmatrix}$$

and α= TE or TM.

For the TE_{mn} or TM_{mn} mode, the elements of the matrix L_i become $L_{1mn\alpha}$ and $L_{2mn\alpha}$, which they have the following partitioned form,

$$l_{1mn\alpha}=\frac{\left(Z_{mni\alpha}^2-z_{0i}^2\right)\sinh\left(\gamma_{mni}h_i\right)}{\Delta_c} \text{ and } l_{2mn\alpha}=\frac{2Z_{mni\alpha}z_{0i}}{\Delta_c}$$

where: $Z_{mniTE}=\dfrac{j\omega\mu_0}{\gamma_{mni}}$, $Z_{mniTM}=\dfrac{\gamma_{mni}}{j\omega\varepsilon_0\varepsilon_{ri}}$,

$$\Delta_c=2Z_{mni\alpha}z_{0i}\cosh\left(\gamma_{mni}h_i\right)+\left(Z_{mni\alpha}+z_{0i}^2\right)\sinh\left(\gamma_{mni}h_i\right)$$

$$\gamma_{mni}=\sqrt{\beta_{xm}^2+\beta_{yn}^2-k_0^2\varepsilon_{ri}}\,,\ k_0=\omega\sqrt{\mu_0\varepsilon_0}\,,\omega=2\pi\frac{c}{\lambda}$$

$$\beta_{xm}=\beta_x+\frac{2m\pi}{a}\ \beta_{yn}=\beta_y+\frac{2n\pi}{b},$$

$$\beta_x=\omega\sqrt{\varepsilon_{r1}\mu_{r1}}\sqrt{\varepsilon_0\mu_0}\sin\theta\cos\phi\ ,$$

$$\beta_y=\omega\sqrt{\varepsilon_{r1}\mu_{r1}}\sqrt{\varepsilon_0\mu_0}\sin\phi\cos\theta\,.$$

a and b are respectively the periodicity along (ox) and (oy), θ and φ define the angle of incidence.

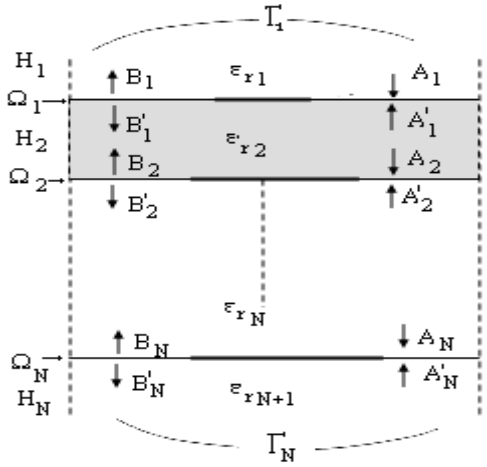

Fig. 3. Definition of waves for the multilayer structure.

On the upper and lower parts of the multilayer structure (medium 1 and medium N), the higher-order modes are shunted by their reactive impedance Z_i, which relates the tangential electric field E_{Ti} to the total current density J_i. Consequently, we obtain,

$$E_{Ti}= Z_i J_i\,. \tag{6}$$

Thus, with equation (2), we can define a reflection operator in modes. Hence, we deduce the reflected spectral wave A_i from the incident spectral B_i as,

$$\left\{A_i=\hat{\Gamma}_i\,B_i\right\}_\alpha \tag{7}$$

$\hat{\Gamma}_{i\alpha}=\dfrac{Z_{mni\alpha}-z_{0i}}{Z_{mni\alpha}+z_{0i}}$, α=TE or TM and i=1 ,or N.

Consequently, with equations (5) and (7), we deduce that the global spectral equation relates the diffracted wave A_i to incident wave B_i in the spectral domain.

$$\left\{\begin{vmatrix}A_1\\A_1'\\A_2\\\vdots\\A_{i-1}'\\A_i\\\vdots\\A_n'\end{vmatrix}=\begin{vmatrix}\Gamma_1 & & & & & & \\ & [L_2] & & & & & \\ & & \ddots & & & & \\ & & & [L_i] & & & \\ & & & & \ddots & & \\ & & & & & \Gamma_N\end{vmatrix}\begin{vmatrix}B_1\\B_1'\\B_2\\\vdots\\B_{i-1}'\\B_i\\\vdots\\B_n'\end{vmatrix}+\begin{Bmatrix}A_{00}\\0\\0\\\\0\\0\\\\0\end{Bmatrix}\right\}_\alpha \tag{8}$$

In the above equation, we have included the excitation wave $A_{00}=\begin{vmatrix}A_{ox}\\A_{oy}\end{vmatrix}$. A_{00} is defined in the spectral domain and has the following expression:

For TE polarization:

$$\begin{cases}A_{0x}=\dfrac{1}{2\sqrt{Z_{oi}}}\dfrac{\beta_y}{\sqrt{|\beta_x|^2+|\beta_y|^2}}\dfrac{1}{\sqrt{ab}}e^{-j(\beta_x x+\beta_y y)}\\ A_{0y}=\dfrac{-1}{2\sqrt{Z_{oi}}}\dfrac{\beta_x}{\sqrt{|\beta_x|^2+|\beta_y|^2}}\dfrac{1}{\sqrt{ab}}e^{-j(\beta_x x+\beta_y y)}\end{cases}. \tag{9}$$

For TM polarization:

$$\begin{cases}A_{0x}=\dfrac{-1}{2\sqrt{Z_{oi}}}\dfrac{\beta_x}{\sqrt{|\beta_x|^2+|\beta_y|^2}}\dfrac{1}{\sqrt{ab}}e^{-j(\beta_x x+\beta_y y)}\\ A_{0y}=\dfrac{1}{2\sqrt{Z_{oi}}}\dfrac{\beta_y}{\sqrt{|\beta_x|^2+|\beta_y|^2}}\dfrac{1}{\sqrt{ab}}e^{-j(\beta_x x+\beta_y y)}\end{cases}. \tag{10}$$

Equations (9) and (10) are derived from the characteristic functions of periodic waveguide.

The implementation of the iterative procedure consists in establishing a recursive relationship between the two spatial and spectral equations, respectively equations (4) and (8).

In addition, this iterative procedure has an alternative behavior between the spatial (on the circuit) and spectral domain (in the two sides). At each iteration, it is necessary to change the type of domain. In the present study, we combine the Wave Concept with the 2D-FFT algorithm, which is called Fast Mode Transformation FMT [15]. The iterative procedure is summarized in Fig. 4. A successive set of iteration is considered to determine a relationship between (k) and (k+1) interaction waves. This is illustrated in the following way.

First, we take the spectral equation (8) and deduce the spectral incident waves $(A_i)_{TE,\,TM}$. In the same iteration, we take the IFMT transformation (Inverse Fast Mode Transformation) to calculate the spatial waves, this transformation is expressed as,

$$\begin{vmatrix} A_x \\ A_y \end{vmatrix}^k = [T]^{-1} \cdot \begin{vmatrix} IFFT_{2D}(A_{TE}) \\ IFFT_{2D}(A_{TM}) \end{vmatrix}^k \qquad (11)$$

The matrix [T] is the transformation matrix from the classical 2D-FFT to 2D-FFT in modes, which is derived from periodic waveguide chrematistic functions and has the following partitioned form,

$$[T] = \begin{vmatrix} N_{ymn} & -N_{xmn} \\ N_{xmn} & N_{ymn} \end{vmatrix} \qquad (12)$$

with $N_{xmn} = \dfrac{1}{\sqrt{ab}} \cdot \dfrac{\beta_{xm}}{\sqrt{|\beta_{xm}|^2 + |\beta_{yn}|^2}}$

and $N_{ymn} = \dfrac{1}{\sqrt{ab}} \cdot \dfrac{\beta_{yn}}{\sqrt{|\beta_{xm}|^2 + |\beta_{yn}|^2}}$

a, b, β_{xm} and β_{yn} are defined in equation (5).

The second step consists in taking the spatial equation (4) and deducing the reflected spatial wave (Bi)x,y from the incident (Ai)x,y.

In the third step, we come back to the spectral domain using the direct FMT. This should be done as follows,

$$\begin{vmatrix} B_{TE} \\ B_{TM} \end{vmatrix}^{k+1} = [T] \begin{vmatrix} FFT_{2D}(B_X(x,y)) \\ FFT_{2D}(B_Y(x,y)) \end{vmatrix}^k \qquad (13)$$

Finally, we calculate the scattered matrix parameters, and then we test the convergence and return to the fist step if the convergence is not obtained.

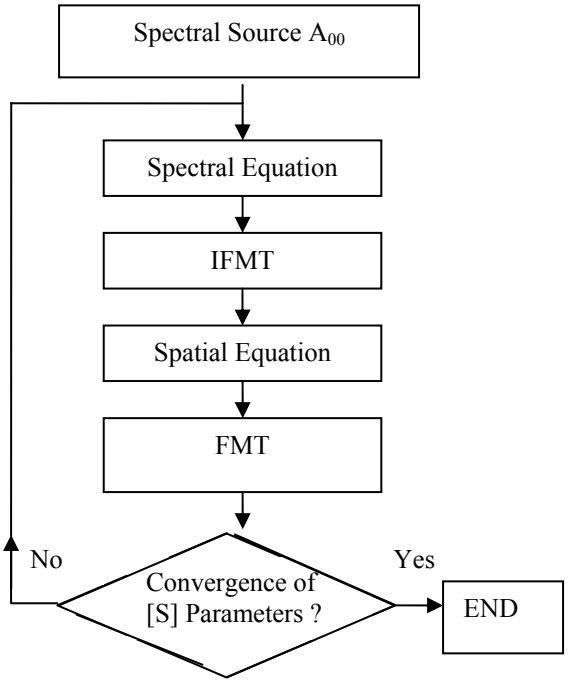

Fig. 4. Schematic description of the iterative process.

III. APPLICATIONS

To evaluate the numerical complexity procedure described in section II, we will make a comparison with the Method of Moments MoM. In terms of the WCIP method, the numerical complexity depends on the interfaces number and the spatial mesh of the circuit plane, whereas in the classical Method of Moments MoM, this complexity depends on the rate of metallization [16]. In order to compare the numerical complexity of these two methods, let us consider Q as the number of cells meshing the whole interface and Q_m the number of cells on the metallic domain. Q_m corresponds to the number of rooftops in the MoM. For the WCIP, the total number of operations for T iterations is $Oper_{WCIP} = 4QT\left(1+3\log_2 Q\right)$ and for the MoM is $Oper_{MoM} = Q^3/3R^3$ where $R = Q/Q_m$ [12]. Figure 5 shows the evolution of the operation numbers as the metallic rate function. The intersection point 'M' of the two curves corresponds to 30% of metallization and 0.9011 107 operations, is calculated with 32x32 cells and 200 iterations. We see that the WCIP is very speedy if the metallization is as large as in the FSS structures.

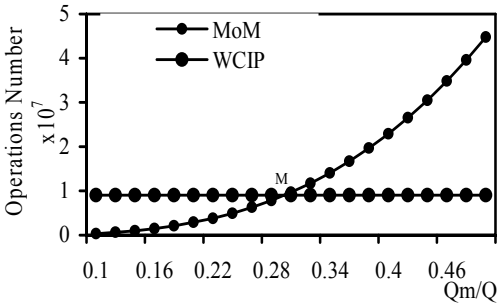

Fig. 5. Comparison in number of operations.

The convergence of the resonance frequency as mesh size thinness Δ is studied. Figure 6 shows that before the convergence, the resonant frequency increases if Δ decreases. At the convergence, the resonance frequency is about 10.3 GHz, is obtained from Δ=0.2 mm. In this study, the source excitation used in this application is the fundamental TM mode with normal incidence *(θ = φ = 0)*.

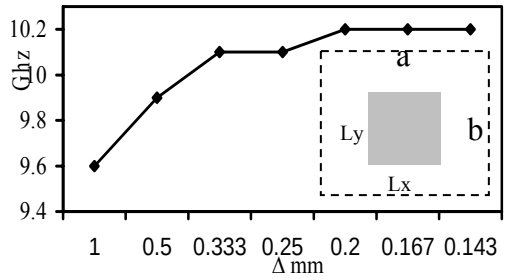

Fig. 6. Convergence of resonance frequency as function of mesh size thinness Δ where: h = 3mm, ε_r =3.5, a = b = 20 mm and $L_x = L_y$ =10 mm.

In order to validate our method, we consider again the structure of Fig. 6. The results of our method are compared to those calculated with Method of Line [17] and depicted in Fig. 7. In the two cases, a good agreement is obtained between results.

The second example consists in studying two layers structure as shown in Fig. 8. A TM source with arbitrary incidence is considered in this application.

The physical parameters are:

$$\begin{cases} a = 0.5\lambda_0, \quad b = 0.5\lambda_0 \\ \text{Plate}: L_x^P = 0.131\lambda_0, \quad L_y^P = 0.15\lambda_0 \\ \text{Slote}: L_x^f = 0.001\lambda_0, \quad L_y^f = 0.115\lambda_0 \\ f = 15\text{GHz}, \; h = 0.002\lambda_0, \; \varepsilon_r = 12.8 \end{cases}$$

Three cases of ϕ are studied: E-plane ($\phi = 0$), D-plane ($\phi = 45^o$)and H-plane ($\phi = 90^o$). In the case of E-plane the evolution of power reflection coefficient as function of θ is plotted in Fig. 9. At all range of θ, a good agreement is observed between our results and measured data [17], a maximum discrepancy is less than 2 %. The total reflection is observed for $\theta = 83^o$.

In the two other cases [D-plane] and [H-plane], the power reflection variation is plotted, respectively in Figs. 10 and 11. Only measured data [18] presents a total reflection at the predicted angle. In our simulation, the total reflection is 0.73 in D-plane and ≈ 0.865 in H-plane. The discrepancy is due to mode excitation. In practice, [17], the excitation is realized by coaxial cable. Then, a field of symmetric cylindrical is produced and the TM mode is coupled at all directions.

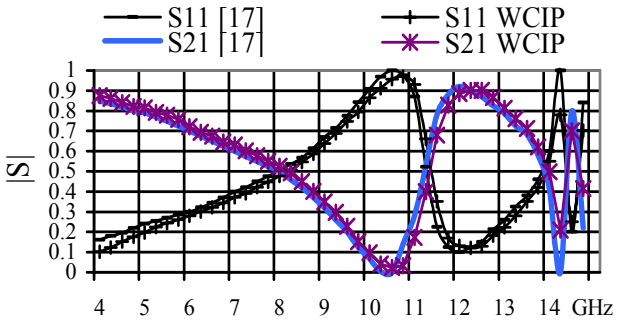

Fig. 7. Power coefficients S_{11}^2 and S_{21}^2as function of frequency where: h = 3mm, ε_r=3.5. a = b = 20 mm and $L_x = L_y$ =10mm.

a: Side View

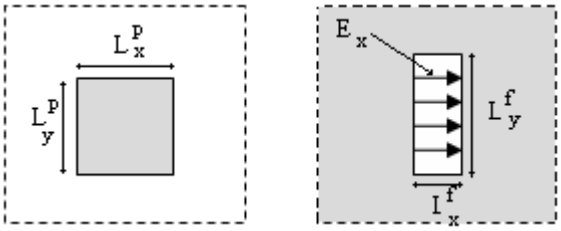

b: Interface Ω_1 c: Interface Ω_2

Fig. 8. Slot coupled periodic antenna.

IV. CONCLUSION

In this paper, the transverse wave concept iterative procedure FMT-WCIP is proposed for the analysis of the frequency selective surface (FSS) with arbitrary angle of excitation. The numerical complexity is studied and compared to the classical MoM. As a result, a minimum computation time is required and the number of operations is reduced by using the FMT based on the 2D-

FFT algorithm. The comparison between the simulation and the measurement results has proved the efficiency of our proposed design procedure of a simple and multilayer FSS.

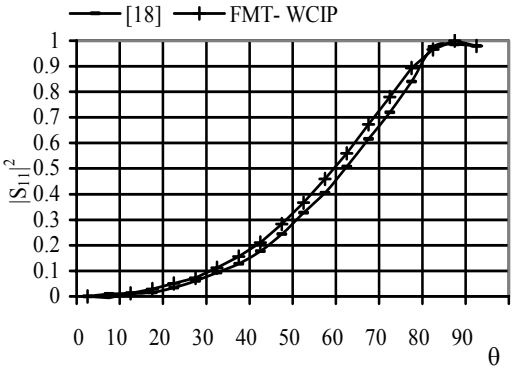

Fig. 9. Amplitude of power reflection coefficient versus θ for E-plane.

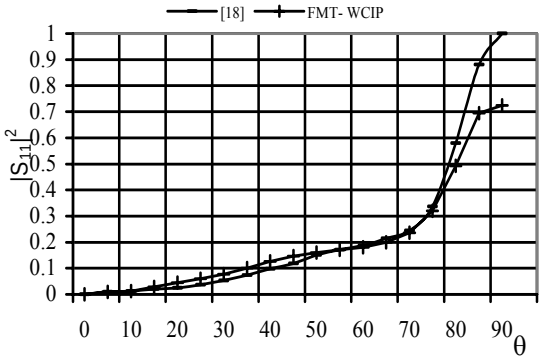

Fig. 10. Amplitude of power reflection coefficient versus θ for D-plane.

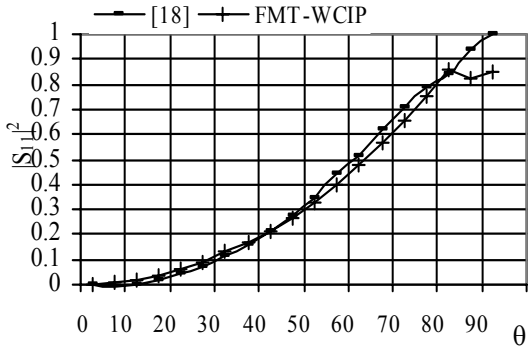

Fig. 11. Amplitude of power reflection coefficient versus θ for H-plane.

REFERENCES

[1] B. A. Munk, *Frequency Selective Surfaces: Theory and Design*, Wiley, New York, 2000.

[2] D. J. D. H. Werver, A. Monorchio, L. Lanuzza, and M. J. Wilhelm, "The design synthesis of multi-band artificial magnetic conductors using high impedance frequency selective surfaces," *IEEE Trans. Antennas Propag.,* vol. 53, no.1, pp. 8-17, Jan. 2005.

[3] D. Hokim and J. Ick Choi, "Design of a multi-band frequency selective surface," *ETRI Journal*, vol. 28 no. 4, Aug. 2006.

[4] N. Bliznyuk and N. Engheta, "Numerical study of polarization dependant focusing for a bi-layer planar FSS reflective at millimeter wave length," *Microwave and Optical Technology Letters,* vol. 40, no. 5, pp. 361-365, Mar. 2004.

[5] A. K. Bhattacharyya, "A numerical model for multilayered microstrip phased-array antennas," *IEEE Trans. Antennas Propag*, vol. 44, no. 10, pp. 1386–1393, Oct. 1996.

[6] M. Bozzi, L. Perregrini, J. Weinzierl, and C. Winnewisser, "Efficient analysis of quasi-optical filters by a hybrid MoM/BI-RME method*," IEEE Trans. Antennas Propag*., vol. 49, no. 7, pp. 1054–1064, Jul. 2001.

[7] G. Zarrillo and K. Aguiar, "Closed-form low frequency solutions for electromagnetic waves through a frequency selective surfaces," *IEEE Trans. Antennas Propag.*, vol. 35, pp. 1406–1417, Dec. 1987.

[8] J. Jin and J. L. Volakis, "Electromagnetic scattering by a perfectly conducting patch array on a dielectric slab," *IEEE Trans. Antennas Propag.*, vol. 38, no. 4, pp. 556–563, 1990.

[9] Zhi Liang Wang, Kozo Hashimoto, Naoki Shinohara, and Hiroshi Matsumoto, "Frequency-Selective Surface for Microwave Power Transmission*," IEEE Trans. MTT,* vol. 47, no.10, Oct. 1999.

[10] R. J. Langley and E. A. Parker, "Equivalent circuit model for arrays of square loops," *Electron. Letters*, vol. 18, pp. 294–296, 1983.

[11] N. Sboui, A. Gharsallah, A. Gharbi, and H. Baudrand, "Analysis of double loop meander line by using iterative process," *Microwave and Optical Technology Letters,* vol. 26, pp. 396-399, June 2000.

[12] N. Sboui, A. Gharsallah, H. Baudrand, and A. Gharbi, "Design and modeling of RF MEMS switch by reducing the number of interfaces*," Microwave and Optical Technology Letters*, vol. 4913, no. 5, pp. 1166-1170, May 2007.

[13] N. Sboui, A. Gharsallah, A. Gharbi, and H. Baudrand, "Global modeling of microwave active circuits by an efficient iterative procedure," *IEE Proc. Microw. Antennas Propag.* vol. 148, no. 3, pp. 209-212, June 2001.

[14] M. Azizi, M. Boussouis, H. Aubert, and H. Baudrand, "A Three-dimensional Analysis of Planar Discontinuities by an Iterative Method," *Microwave and Optical Technology Letters*, vol. 13, no. 6, pp. 372-376, Dec. 1996.

[15] M. Tiataouine, A. G. Neto, H. Baudrand, and F. Djahli, "Analysis of frequency selective surface on isotropic/anisotropic layers using WCIP method," *ETRI Journal,* vol. 29, no. 1, Feb. 2007.

[16] R. Mittra, H. Chan, and T. Cwik, "Techniques for analysis frequency selective surfaces-A Review," *Proceeding of the IEEE,* vol. 76, no. 12, Dec. 1988.

[17] E. Choinière and J. J. Laurin," Modeling of planar multilayer periodic arrays using the method of lines," *ACES Journal,* vol. 17, no. 2, July 2002.

[18] D. M. Pozar and D. H. Schaubert, "Analysis of an infinite array of rectangular microstrip patches with idealized probe feeds," *IEEE Trans. Antennas Propag.,* vol. 32, no. 10, pp. 1101–1107, Oct. 1981.